ELSEVIER

Ceramics International 32 (2006) 575–581

CERAMICS INTERNATIONAL

www.elsevier.com/locate/ceramint

Fabrication and mechanical properties of ultra-fine grained γ-Ni–20Fe/Al_2O_3 composites

X.Y. Qin [a,b,*], R. Cao [b,c], H.Q. Li [c]

[a] School of Science, Hefei University of Technology, 230009 Hefei, PR China
[b] Key Laboratory of Materials Physics, Institute of Solid State Physics Chinese Academy of Sciences, 230031 Hefei, PR China
[c] School of Materials Science and Engineering, Hefei University of Technology, 230009 Hefei, PR China

Received 12 January 2005; received in revised form 2 February 2005; accepted 4 April 2005
Available online 3 June 2005

Abstract

High-dense (relative density $D \geq 98\%$) ultra-fine grained γ-Ni–20Fe/Al_2O_3 composites were fabricated by using a mechano-chemical process plus hot-pressing. Microstructure investigations revealed that fine γ-Ni–20Fe particles with the dimensions of several hundreds of nanometers dispersed homogeneously at the matrix grain boundaries. Mechanical tests indicate that fracture toughness increases monotonously from 4.7 MPa $m^{1/2}$ for monolithic alumina to 8.4 MPa $m^{1/2}$ for ~19 vol.% Ni–20Fe/Al_2O_3 composites. Fracture strength σ_f increased with addition of Ni–20Fe phase as Ni–20Fe content was low (≤5 vol.%). However, σ_f decreased with further increase of Ni–20Fe content, exhibiting a maximum strength of ~600 MPa at ~5 vol.% Ni–20Fe. The improvement of the mechanical properties could be ascribed to the microstructure refinement of the composites and increase of cracking resistance introduced by the dispersed Ni–Fe phase, which was supported by fracture characteristic observations.

Keywords: Hot-pressing; B. Composites; C. Mechanical properties; D. Al_2O_3

1. Introduction

Metal/ceramic-based ultra-fine grained composites or nanocomposites in which nanometre-sized particles having a diameter from a few to several hundreds of nanometers are incorporated into ceramic matrices [1] are attractive because of their great potentials in improving the toughness of monolithic ceramics. Many efforts have been made on these nanocomposites. For instance, Ni/Al_2O_3 nanocomposite [2] was reported to have improved mechanical properties as well as attractive magnetic properties, which suggested their talent functional applications. Later, Fe/Al_2O_3 [3] and Ni–Co/Al_2O_3 [4] nanocomposites were successfully synthesized and their mechanical properties were explored.

The present work focused on γ-Ni–*x*Fe/Al_2O_3 composite system. γ-Ni–*x*Fe alloys with *x* being in the range of 10–65 wt.%, so called Permalloy, are important soft magnetic materials [5–8], which have been widely used in industry for things such as recording heads, transformers or magnetic shielding materials [5]. Besides, γ-Ni–*x*Fe alloys possess f.c.c. crystallographic structure with good ductility, and their thermal expansion coefficient changes with *x* [5], which suggests that, as a disperse phase, Ni–*x*Fe alloys can thermally match ceramic matrices if their compositions are chosen properly. Therefore, once they are incorporated into alumina, they could not only improve the toughness of monolithic alumina, but also introduce soft magnetism into the composite system, realizing the combination of superior mechanical properties with excellent magnetic performance. In this report, γ-Ni–20Fe/Al_2O_3 ultra-fine grained composites or nanocomposite were fabricated and its mechanical properties were investigated. A study on magnetic properties of γ-Ni–

* Corresponding author. Tel.: +86 5515592750; fax: +86 5515591434.
E-mail address: xyqin@issp.ac.cn (X.Y. Qin).

0272-8842/$30.00
doi:10.1016/j.ceramint.2005.04.013

20Fe/Al_2O_3 and the effects of different Ni–*x*Fe alloys (with different *x*) on properties of Ni–*x*Fe/Al_2O_3 will appear elsewhere [9].

2. Experimental procedures

Commercially available nanometer-sized alumina (purity ≥99.99%) was wet ball milled in 200 ml alcohol for 5 h with high-purity Al_2O_3 balls to break up the agglomerates in high-energy ball-milling machine. The ball-to-powder ratio was 6:1 and the rotation speed was 250 r/h. The ball-milled alumina was sieved in 200-items sieve as the source material after dried at 60 °C for 24 h. On the other hand, high-purity $Fe(NO_3)_3{\cdot}H_2O$, $Ni(NO_3)_2{\cdot}H_2O$ powders were used as a source material for Ni–Fe. The composition of Ni–Fe alloy was Ni–20 at.% Fe. The Ni–20Fe contents in four different composites are 5, 9, 15 and 19 vol.%, respectively. Weighted powders were initially dissolved in 200 ml alcohol and then mixed with the ball-milled Al_2O_3 for 5 h. After dried at 60 °C for 24 h, the mixture was sieved in 200-items sieve, and then calcined at 500 °C in air for 2 h. In order to obtain composites with homogeneously dispersed particles and crush soft agglomerates of the calcined powder, the calcined powders were wet ball milled again in 200 ml alcohol for 4 h, and then dried and sieved as above. The re-milled powders were subsequently reduced at 600 °C for 2 h to form nanometer sized γ-Ni–20Fe alloy (hereafter refer to it as Ni–Fe) in situ. Bulk samples with size of ϕ 60 mm × (∼) 3.5 mm were obtained by hot-pressing at 1400 °C for 40 min under applied stress of 30 MPa in high purity (5 N) argon atmosphere. For comparison, a monolithic alumina sample was prepared under the identical condition.

The hot-pressed samples were ground, polished and finally cut into rectangular shaped specimens with 4 mm × 3 mm × 35 mm in size for bending tests. Sample phases were analysed with X-ray diffraction. Microstructures of powders were examined with transmission electron microscopy (TEM) and the Brunauer-Emmett-Teller (BET) method with nitrogen absorption. To reveal the grain morphologies and dispersion states of the composites, Ni–20Fe/Al_2O_3 and monolithic alumina specimens were thermally etched for 15 min at 1200 and 1400 °C, respectively. The morphology of thermally etched surfaces and fractography of bulk specimens were observed with field-emission-scanning electron microscopy (FE-SEM). Sample compositions were confirmed with energy dispersive X-ray spectroscopy (EDS). The densities of the hot-pressed specimens were measured based on Archimedes principle in alcohol with the accuracy of ±0.5%. Vickers indentation tester was used to measure the hardness (load: 1.96 N; loading time: 30 s) and fracture toughness of the specimens (load: 98 N; loading time: 15 s), for which at least six indentations were conducted. Fracture strength was obtained by three-point bending tests (span: 30 mm) of, at least, five specimens with a cross-head speed of 0.5 mm/min.

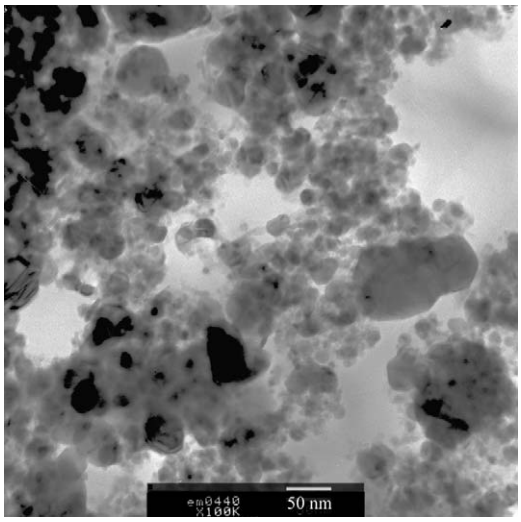

Fig. 1. TEM micrograph for the 15 vol.% Ni–20Fe/Al_2O_3 nanocomposite powder.

3. Results

3.1. Microstructures

The average particle sizes for powder samples with different Ni–Fe contents, after hydrogen reduction, were determined to be 13–50 nm. Fig. 1 gives a TEM micrograph that shows the particle morphologies for the 15% Ni–20Fe/Al_2O_3 powder. One can see that most of particles have sizes in the range from ∼10 to ∼40 nm with light agglomeration, which is beneficial to densification during subsequent hot-pressing. Table 1 lists the densities and compositions of the bulk samples. One can see that the relative densities of all samples are ≥98%. Although sample density differs a little for samples with different Ni–Fe contents, no clear relationship between density and the composition was found.

Fig. 2 shows XRD patterns for S1 and S2. As compared to the pattern of S1, there are some additional reflection peaks in the pattern of S2 that are consistent exactly with those peaks originating from γ-Ni–Fe alloy (as marked in the figure), indicating that there are only two phases in S2: one is γ-Ni–Fe and the other is α-Al_2O_3. In fact, apart from the two constituent phases, no other phase such as Fe, Ni or corresponding metal oxides was observed for all the composite samples with different compositions. This result indicates that Ni- and Fe-nitrates have been completely

Table 1
The Ni–20Fe content (*C*), absolute density (ρ), and relative density (*D*) for different samples after hot-pressing

	Sample				
	S1	S2	S3	S4	S5
C (vol.%)	0	5	9	15	19
ρ (g/cm^3)	3.91	4.17	4.36	4.66	4.86
D (%)	98.3	98.7	99.0	98.4	98.0

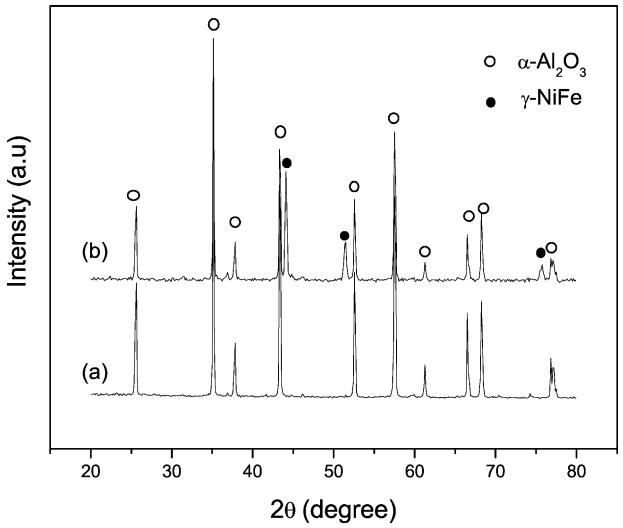

Fig. 2. XRD patterns of (a) monolithic α-Al_2O_3 (S1), and (b) 5 vol.% Ni–20Fe/Al_2O_3 composite (S2).

converted to Ni–Fe alloy, and all the composites are composed entirely of γ-Ni–Fe and α-Al_2O_3.

In order to reveal the dispersion states of the alloy phase in the composite samples, FE-SEM observations on the thermally etched sample surfaces were carried out (Fig. 3). Fig. 3a shows that the microstructure of the monolithic α-Al_2O_3 (S1) consists of both large grains with several micrometers and smaller grains with several hundred nanometers. Specially, some small grains with ∼100–200 nm can still be found (see the inset in Fig. 3a) in some location. The existence of these small grains would affect its mechanical properties positively (see next section). On the other hand, one can see from Fig. 3b and c that Ni–Fe alloy particles in the composites were dispersed fairly homogenously in the matrix. Since the temperature in thermally etching composite samples (1200 °C) is 200 °C lower than that in etching monolithic alumina sample (a lower temperature is necessary in etching the composite samples to exhibit disperse state of the alloy particles, for as the temperature is higher than 1200 °C, 1400 °C for instance, the alloy particles would merge together on a large scale due to over-heating), the grain boundaries of the alumina matrix in the composites are not as clear (under FE-SEM) as those in monolithic alumina sample. However, by careful checking Fig. 3b and c one finds that matrix grains with sizes of near 1 μm or less prevail for the composites. It should be noted that the observed large domains on the composite sample surfaces, such as that as marked by a square in the Fig. 3b, are not single grains of the matrix. In fact, they display granular

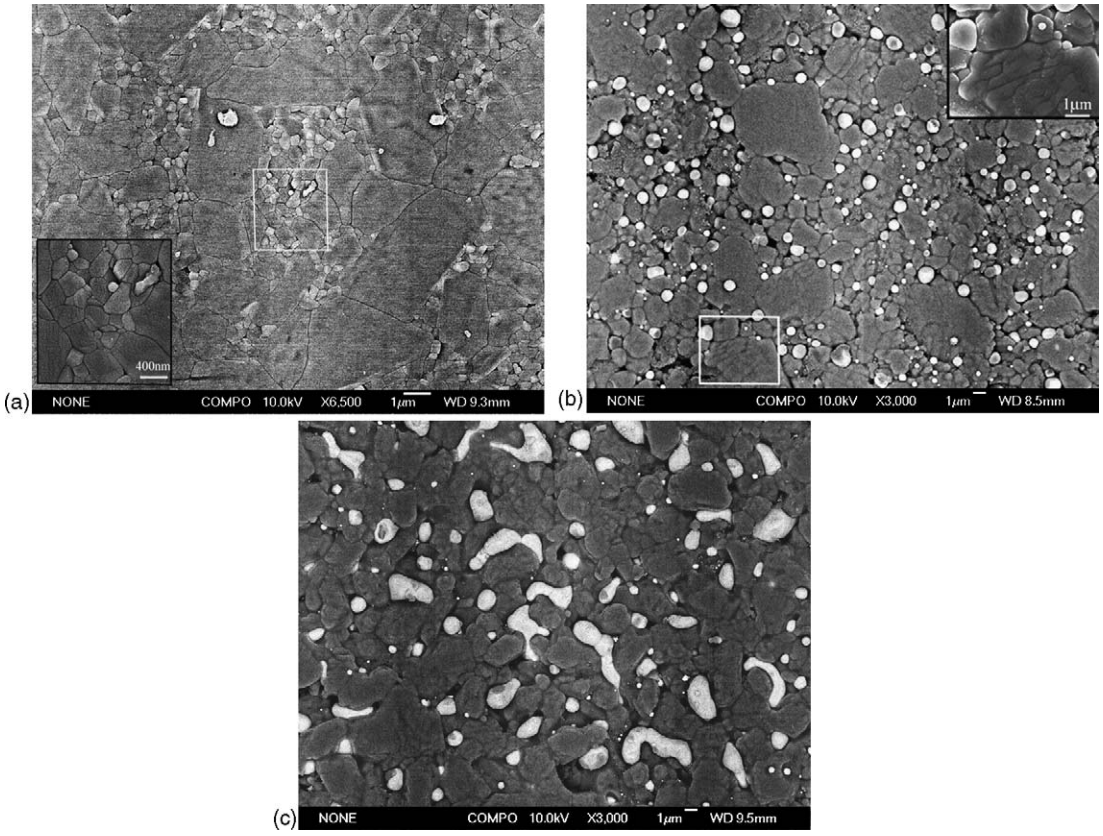

Fig. 3. FE-SEM micrographs of thermally etched (at 1200 °C for 15 min) sample surfaces for (a) monolithic α-Al_2O_3, where the inset in the left-bottom corner shows the magnified image of the region in the square, (b) 5 vol.% Ni–20Fe/Al_2O_3 composite, where the inset in the up-right corner shows the magnified micrograph of the domain in the marked square, and (c) 15 vol.% Ni–20Fe/Al_2O_3 composite.

structure. The inset in up-right corner of Fig. 3b shows a magnified micrograph for the domain within the marked square. One can see that the domain is actually aggregates of the matrix grains, being composed of many grains with dimensions of sub-micrometers. All the observations show that main and important microstructural difference between monolithic Al_2O_3 and the composites is that the matrix grain sizes of the composites are more homogenous and, on the average, are clearly smaller than those of monolithic Al_2O_3, indicating that addition of Ni–Fe nanoparticles inhibited the grain growth of alumina matrix effectively.

On the other hand, few large voids or porosities were spotted on the sample surfaces of either monolithic alumina or the composites, being consistent with measured high densities of the samples (Table 1). The small voids present on the thermally etched surfaces of the composite (see Fig. 3b) were, however, presumably produced during the thermally etching process: where Ni–Fe particles could diffuse out and merge with other Ni–Fe particles on the surface during etching process. The mergence of the Ni–Fe particles can be seen more clearly in Fig. 3c that shows large irregular Ni–Fe agglomerates appearing on the surface due to small spacing among particles (because of higher Ni–Fe content as compared to S2). In other words, the observed sizes of the Ni–Fe particles on the etched surfaces do not represent actual particle sizes in interior of the composites, implying that the particle sizes of the Ni–Fe dispersing phase in interior of the composites are actually smaller than those being observed on the thermally etched surface, which is confirmed in fractography (Fig. 8b).

3.2. Mechanical properties

Fig. 4 gives the plots of fracture strength and Vickers hardness versus Ni–Fe content. One can see that Vickers hardness decreases monotonously from ~20 GPa (Al_2O_3) to ~14 GPa as Ni–Fe content increases from 0 to 19 vol.%. However, fracture strength, σ_f, shows non-monotonous behaviour: it rises first from ~540 to 600 MPa as Ni–Fe

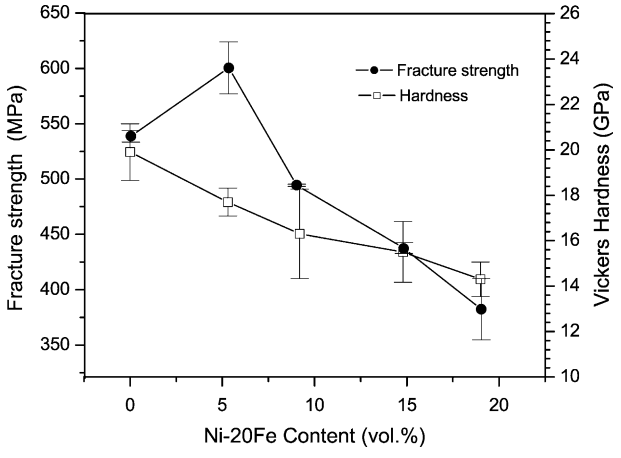

Fig. 4. Plots of fracture strength and Vickers hardness vs. Ni–20Fe content.

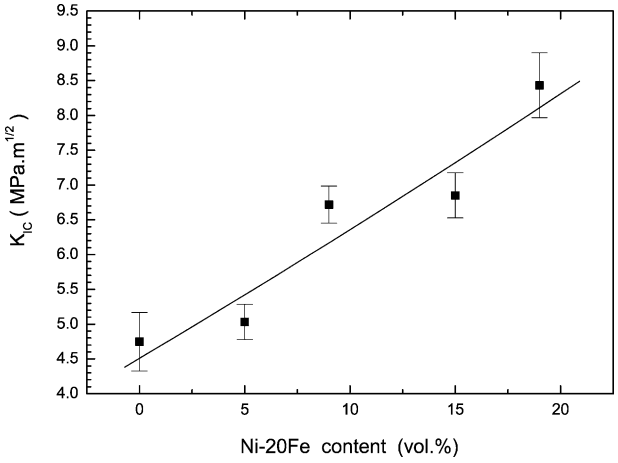

Fig. 5. Plot of fracture toughness K_{1C} vs. Ni–20Fe content.

content increases from 0 to ~5 vol.%, and then decreases as Ni–Fe content increases further, exhibiting a peak at around 5 vol.% Ni–Fe in the plot of σ_f versus Ni–Fe content.

In contrast to fracture strength, fracture toughness of the composite increases monotonically with increasing Ni–Fe content (see Fig. 5). The fracture toughness K_{1C} is calculated according to following equation given by Niihara et al. [10]:

$$K_{1C} = 0.0122\left(\frac{E}{H}\right)^{2/5}\frac{P}{al^{1/2}} \quad (1)$$

where E is the Young's modulus, H is the hardness, P is the indent load, a is the length of half diagonal of the indent, and $l = c - a$ (here c is the length of half indentation crack). As shown in Fig. 5, K_{1C} increases monotonously from 4.7 MPa $m^{1/2}$ for monolithic α-Al_2O_3 to 8.4 MPa $m^{1/2}$ for 19 vol.% Ni–Fe/Al_2O_3, which indicates that the addition of Ni–Fe phase can effectively improve the toughness of alumina.

3.3. Fracture characteristics

The fracture characteristics of the composite were surveyed. Fig. 6a shows an indent as well as cracks produced by indentation around the indent corners (along the diagonal direction from up-left to down-right) for specimen S3. Fig. 6b and c gives magnified micrographs for one of the surface cracks near the indent corner in the right-bottom. One can see from Fig. 6b that the crack propagates along a non-straight trace, and turns its direction frequently during propagation. At much high magnification, however, one finds that the crack deflection occurs mainly at the Ni–Fe particles, as shown by an arrow in Fig. 6c, indicating that the Ni–Fe particles behaviour as obstacles to crack propagation.

Figs. 7 and 8 give FE-SEM micrographs of the fracture surfaces for S1 (Figs. 7a and 8a) and S2 (Figs. 7b and 8b), respectively. It can be seen that the fracture surface of monolithic alumina differs very much from that of S2. The

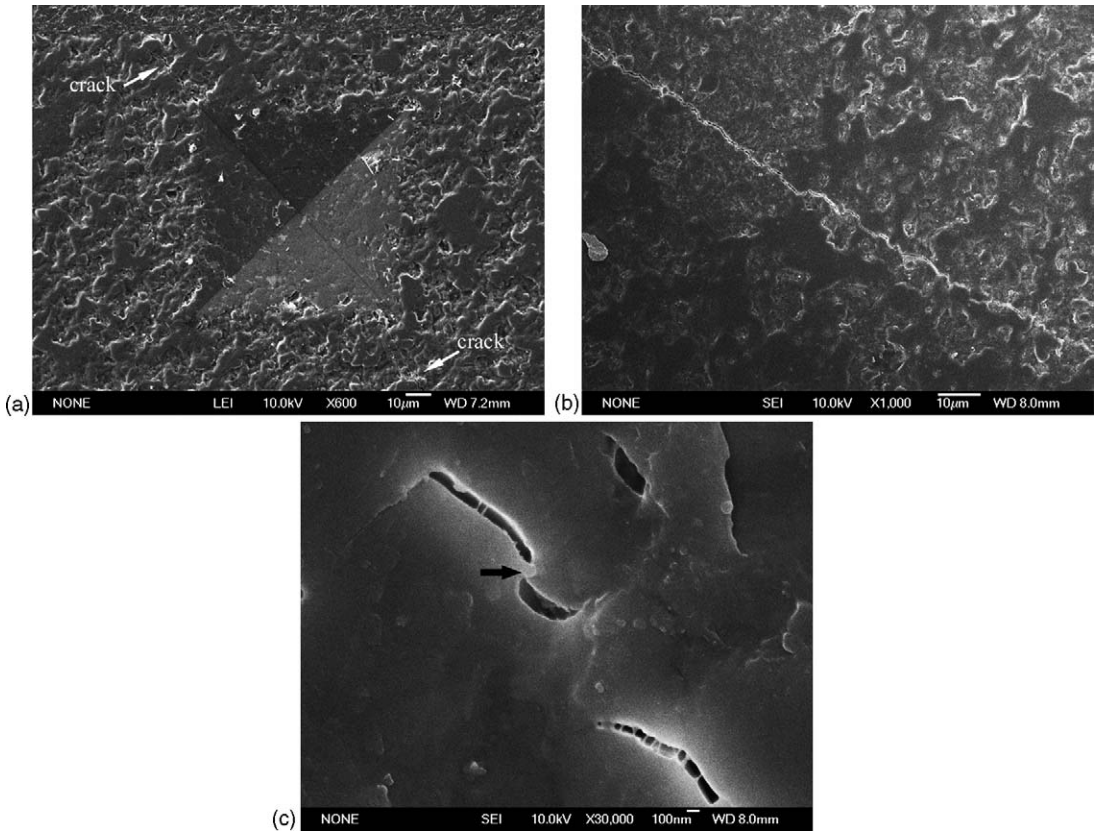

Fig. 6. FE-SEM micrographs for an indent as well as cracks (as shown by the arrows) produced by indentation around the indent corners (along the diagonal direction from up-left to down-right) for specimen S3 (a), a magnified micrograph (with magnification of ×1000) showing that crack propagates along a zigzag-like trace (b), a micrograph with much high magnification (×30,000) which shows crack deflection at a Ni–Fe nanoparticle (c).

fractographs of S1 displayed mixed fracture characteristics: (a) intra-granular cracking occurred for larger (micrometer scale) grains with cleavage steps appearing occasionally, as labelled by letter ''A'' in Fig. 7a; (b) inter-granular cracking that occurred mainly in the region where large number of small (sub-micrometer scale) grains are present (as labelled by letter ''B''), which can be seen more clearly in Fig. 8a. The microstructure of the fracture surface for S2 is much finer and more homogeneous than that for S1 (comparing Fig. 7a with b). From Fig. 8b one can clearly observe that many Ni–Fe particles (with nearly spherical shape) and some pits (where Ni–Fe particles may once occupy) existed on the fracture, indicating that inter-phase failure occurred. In addition, intra-granular failure within the matrix can also be identified, as manifested by appearance of some smooth planes in the fracture surface (Fig. 8b).

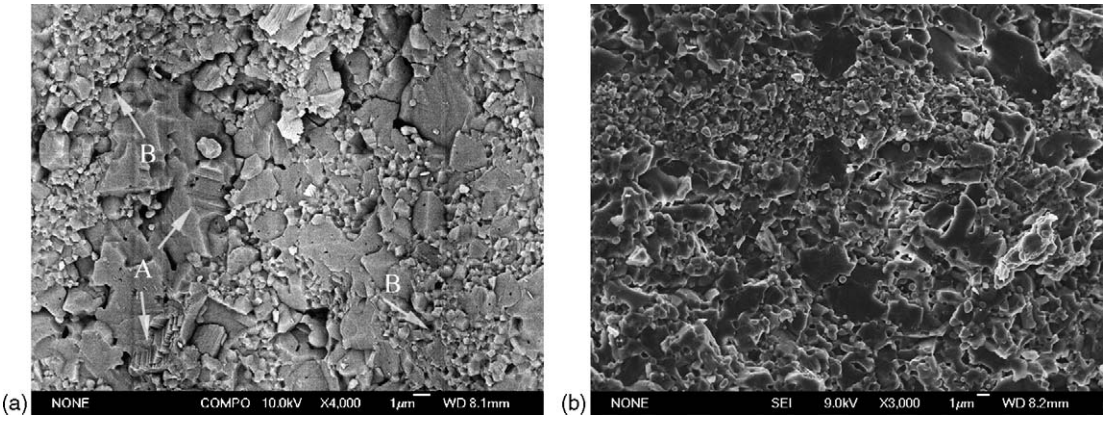

Fig. 7. FE-SEM micrographs of fracture surfaces for (a) monolithic α-Al_2O_3, where letter ''A'' shows the intra-granular failure regions, and ''B'' shows inter-granular failure regions, and (b) 5 vol.% Ni–20Fe/Al_2O_3 composite.

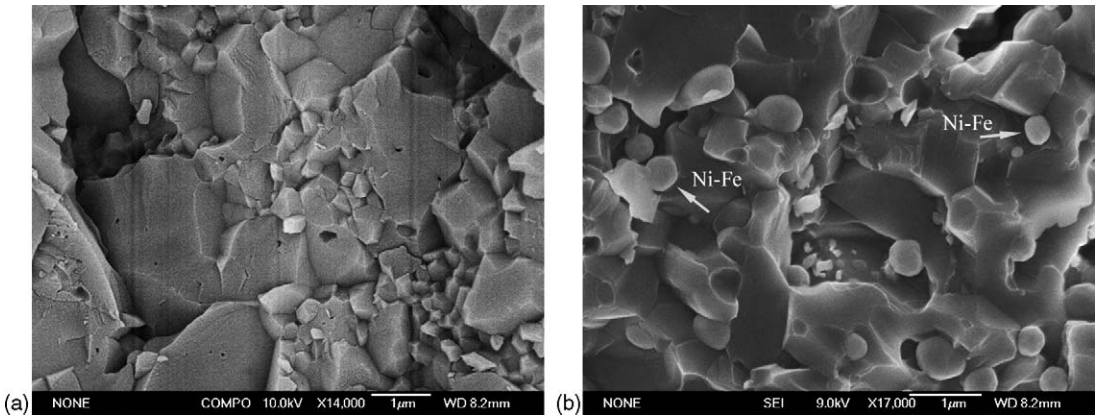

Fig. 8. FE-SEM micrographs of fracture surfaces with high magnifications for (a) monolithic α-Al_2O_3, and (b) 5 vol.% Ni–20Fe/Al_2O_3 composite.

4. Discussions

The toughening of a composite system can be realized through several mechanisms [11], which may include, for instance, microcracking, crack bridging, pull-out of second phase and crack deflection. In the present experiment, cracks were observed to deflect their directions at the dispersed particles as shown in Fig. 6c, which, we believe, is the main reason for fracture toughness increments of the composite system. Since the Ni–Fe phase is much more ductile than the matrix, the stress intensity at the crack tip, as encountered with the alloy particles, is expected to be reduced due to possible plastic deformation of the alloy, leading to halting of crack extension. Further increase of an applied stress is needed to re-initiate the cracking. Moreover, due to ductile nature of γ-Ni–Fe phase, cracking of itself is unlikely to occur, and crack deflection is therefore necessary for further extension of the crack. This crack deflection and its extension around the Ni–Fe particles would lead to inter-phase cracking as observed in Fig. 8b. As the Ni–Fe content increases, the probability of a crack meeting with the ductile particles increases, which would lead to monotonous increase of K_{1C} with Ni–Fe content, as manifested in Fig. 5.

The decrease of the hardness with increasing Ni–Fe content is understandable, considering that the dispersed phase (γ-Ni–20Fe) is much softer than the matrix, and the more of this dispersed phase in the matrix, the softer the composite is. The fracture strength (540 MPa) of monolithic alumina is a little higher than the reported values (350–400 MPa) [12]. This increase in strength may be ascribed to refinement of the microstructures of monolithic alumina (Fig. 3a). The fracture strength, σ_f, of a brittle material is related to its fracture toughness, as measured by the critical stress intensity factor, K_{1C}, through the relationship [13]

$$\sigma_f = Y\frac{K_{1C}}{\sqrt{c}} \quad (2)$$

where c is the half critical crack length, and Y is the geometrical parameter of the flaw. Therefore, an increase in K_{1C} may bring about a higher value of σ_f. This can give an explanation to the increase in the strength of the composite at small Ni–Fe contents (ca. <5 vol.%). That is, the increase in the strength of the composite at the small Ni–Fe content (ca. <5 vol.%) may be produced through toughening mechanism. In addition, critical crack length c is generally proportional to the grain size d in dense polycrystalline materials. As a result, the increased strength of the composites could come partly from the refinement of the matrix grains (this factor would also be the reason for a little higher strength of monolithic alumina than the reported value). However, when Ni–Fe content increased further, as a constituent phase the low strength of Ni–Fe itself would lead to decrease of overall strength of the composite system. Moreover, agglomeration of Ni–Fe particles would form as Ni–Fe increased, which could lower the strength by acting as a fracture source [14]. Both factors could be the reasons that cause fracture strength of the composite system to decrease at higher Ni–Fe content (ca. >5 vol.%).

5. Conclusions

High-dense ultra-fine grained γ-Ni–20Fe/Al_2O_3 composites were fabricated, and their mechanical properties were investigated. Microstructure investigations reveal that fine γ-Ni–20Fe particles with the dimensions of sub-micrometers dispersed homogeneously at the matrix grain boundaries. Mechanical tests indicate that fracture toughness increases monotonously with increasing content of Ni–20Fe in the composition range investigated (from 0 to ∼19 vol.% Ni–20Fe), while fracture strength increased as Ni–20Fe content ≤5 vol.%, and then it decreased with further increasing Ni–20Fe content, exhibiting a maximum strength of ∼600 MPa at ∼5 vol.% Ni–20Fe. The increased strength of the composites can be ascribed mainly to toughening mechanism. While, the fracture toughness increments could be ascribed to the rise of cracking resistance originating from both crack deflection and microstructural refinements of the composite introduced by dispersed ultra-fine Ni–Fe phase.

Acknowledgment

This work was financially supported by Chinese Academy of Sciences through ''Hundred Persons Plan''.

References

[1] R. Roy, Science 238 (1987) 1664.
[2] T. Sekino, T. Nakajima, S. Ueda, K. Niihara, J. Am. Ceram. Soc. 80 (1997) 1139.
[3] J.L. Guichard, O. Tillment, A. Mocellin, J. Mater. Sci. 32 (1997) 4513.
[4] S.T. Oh, M. Sando, K. Niihara, J. Mater. Sci. 36 (2001) 1817.
[5] E.P. Wohifarth (Ed.), Ferromagnetic Materials, vol. 2, North-Holland Publishing Co., Amsterdam, 1980, p. 123.
[6] X.Y. Qin, J.S. Lee, J.G. Kim, J. Appl. Phys. 86 (1999) 2146.
[7] Y. Liu, X.Y. Qin, Chin. Phys. Lett. 20 (2003) 99.
[8] X.Y. Qin, J.G. Kim, J.S. Lee, Nanostructured Mater. 11 (1999) 259.
[9] X.Y. Qin, R. Cao, J. Zhang, H.Q. Li, J. Amer. Ceram. Soc., to be published.
[10] K. Niihara, J. Mater. Sci. Lett. 2 (1983) 221.
[11] K.N. Xia, G.L. Terence, J. Mater. Sci. 29 (1994) 5219.
[12] H.Z. Wang, L. Gao, J.K. Guo, Ceram. Int. 26 (2000) 391.
[13] W.D. Kingery, H.K. Bowen, D.R. Uhlmann, Introduction to Ceramics, 2nd ed., John Wiley & Sons, New York, 1976, p. 765.
[14] M.P. Harmer, S.J. Bennison, C. Narayan, Mater. Sci. Res. 15 (1983) 309.